

Use of solar energy to supply a load by means of a direct current motor-generator

Batassou Guilzia Jeannot¹, Mandeng Jean Jacques², Perabi Ngoffe², and Mane Mane Jeannot¹

¹Laboratory of Computer and Automatic Engineering, UFD of Engineering Sciences. ENSET, University of Douala, Cameroon

²Technology and Applied Sciences Laboratory, Training Unit for Applied Science, University of Douala, Cameroon

Copyright © 2022 ISSR Journals. This is an open access article distributed under the **Creative Commons Attribution License**, which permits unrestricted use, distribution, and reproduction in any medium, provided the original work is properly cited.

ABSTRACT: This paper describes a technique to produce electrical energy by a DC motor-generator set. For the realization of our project, we first optimized the photovoltaic energy by using the MPPT control by fuzzy logic, on a DC/DC converter of Boost type. This photovoltaic energy has an electrical power of 14 kW and will feed the DC motor. The DC motor will drive an alternator up to its nominal speed and will produce an electrical power of 14 kW. The simulation results obtained and presented show the feasibility and efficiency of the proposed technology.

KEYWORDS: DC motor, photovoltaic generator, fuzzy logic, alternator.

1 INTRODUCTION

The ever-increasing variation of oil prices induces relentlessly the increase of the production costs of non-renewable energy. Therefore, extensive research is being done to optimize the capacity of renewable energy sources such as solar energy. The maximum extraction of this solar energy by photovoltaic (PV) cells has already been the subject of several works. Indeed, we find in the literature many MPPT (Maximum Power Point Tracking) control techniques starting from simple techniques like MPPT controllers based on voltage and current feedback [1], [2] to more powerful controllers using algorithms to compute the maximum power point (MPP) of the photovoltaic generator (GPV), among the most used techniques there are P&O (Perturbation and Observation) and IC (Incremental Conductance) [3].

In recent years, more robust control techniques have been associated with MPPT control such as fuzzy logic to increase the efficiency of solar panels. Other controls for solar power optimization have been developed, such as measuring a fraction of short circuit current, or measuring a fraction of open circuit voltage [4], [5]. Some works have been oriented towards the DC motor-alternator architecture. In their studies, AC current was converted to DC current to power the DC motor [6]. This main source being non-stable and non-permanent, the system will experience periods of interruption. In our study, we apply a new technique to make the main source permanent and stable for the operation of our system. This study turns to a double comparative objective. First, the extraction of the maximum power from the photovoltaic (PV) cells by the so-called intelligent control which is based on fuzzy logic on the MPPT controller. Secondly, the production of electrical energy by an alternator driven by a DC motor, which is fed by DC current from the PV cells.

The rest of the paper is organized as follows. In section 2 we describe the methods and materials used, section 3 is devoted to the results, discussions and comments. The article is closed by a conclusion on this study and the perspectives of this work.

2 MATÉRIALS AND MÉTHODES

2.1 ORGANIZATION OF THE STRUCTURE

The structure of our system shown in Figure 1 is essentially made up of the photovoltaic modules, the DC-DC converter plus MPPT device and the DC Motor - Synchronous Alternator group.

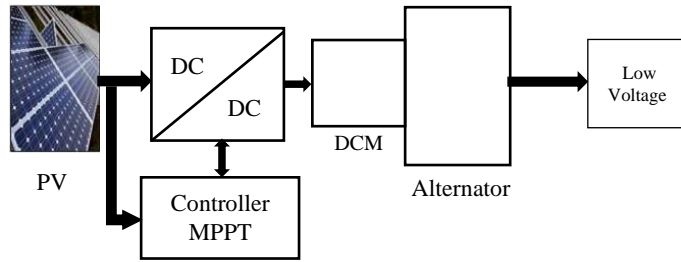


Fig. 1. PV system feeding an DC Motor coupled to an alternator

2.2 OUTPUT POWER OF A PV MODULE

Consider a photovoltaic (PV) module represented by its equivalent diagram given in Figure 2. It consists of a current source modeling the luminous flux, losses modeled by two resistances, the shunt resistance R_{sh} and the series resistance R_s . Finally, appears on this diagram, the diode for the polarization of the cell and the phenomenon of recombination of minority carriers [7], [8]. This model represents the solar cell as a current source that models the conversion of light flow into electrical energy. In recent years, it has been validated that this single-diode model can successfully fit experimental data to some extent [9], [10]. Indeed, this model offers a good compromise between simplicity and accuracy.

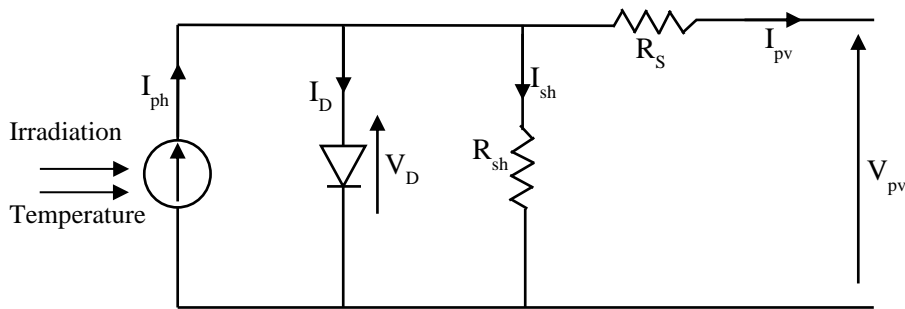


Fig. 2. Equivalent electrical diagram of the single diode model of the solar cell

The experimental conditions of temperature and irradiation are developed as follows:

$$I_{pv} + I_D + I_{sh} = I_{ph} \tag{1}$$

$$I_{pv} = I_{ph} - I_0 \left(\exp\left(\frac{q}{nKT} (V_{pv} + R_s I_{pv})\right) - 1 \right) - \frac{V_{pv} + R_s I_{pv}}{R_{sh}} \tag{2}$$

To obtain the maximum power, the current I_{mp} and the voltage V_{mp} should have their maximum values, i.e.:

$$P_{max,m} = V_{mp} \cdot I_{mp} \tag{3}$$

Using equation (2) for the maximum current value, equation (3) becomes:

$$P_{max,m} = V_{mp} \left[I_{ph} - I_0 \left(\exp\left(\frac{q}{nKT} (V_{mp} + R_s I_{mp})\right) - 1 \right) - \frac{V_{mp} + R_s I_{mp}}{R_{sh}} \right] \tag{4}$$

Therefore, the physical behavior of the photovoltaic module is related to I_0 , R_s and R_{sh} on the one hand, and on the other hand to two other environmental parameters, namely temperature and solar irradiation.

2.3 DC/DC CONVERTER

Our study will exploit the BOOST type DC/DC converter because this converter is the most suitable for PV system. Moreover, it has a simple structure and a higher voltage gain than other converters for a given duty cycle [12]. This DC/DC converter can transform a fixed value DC voltage into an adjustable DC voltage.

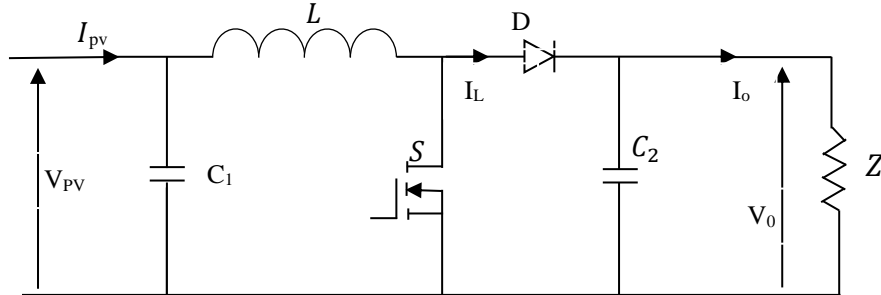


Fig. 3. Electrical diagram of the Boost chopper

This converter is governed by the following equations:

$$V_0 = \frac{1}{1-D} V_{pv} \quad (5)$$

$$I_0 = (1-d)I_L - c_2 \frac{dV_0}{dt} \quad (6)$$

Where D , V_0 and I_0 represent the duty cycle, output voltage and current of the boost converter respectively.

With this converter we will extract the maximum power and run this PV generator at its maximum power point using fuzzy logic on a MPPT (Maximum Power Point Tracking) controller. The voltage and power variation can be translated by equations (7) and (8) and verified by a fuzzy logic algorithm.

$$\Delta P_{pv} = P_{pv}(k) - P_{pv}(k-1) \quad (7)$$

$$\Delta V_{pv} = V_{pv}(k) - V_{pv}(k-1) \quad (8)$$

P_{pv} and V_{pv} are respectively the power and the voltage of the photovoltaic generator at a time k .

➤ MPPT control by fuzzy logic

With the objective of continuously producing the maximum power regardless of the weather conditions (temperature and irradiation), the converter control will place the system at the maximum operating point (Voltage at Maximum Power Point and Current at Maximum Power Point). This fuzzy logic MPPT control is composed of three steps: fuzzification, inference and defuzzification. Figure 4 presents this operating architecture.

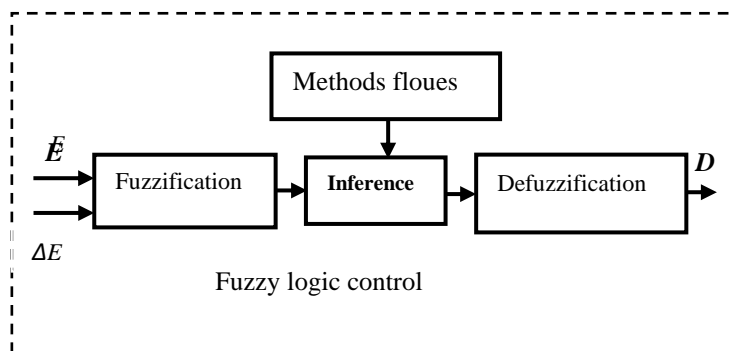


Fig. 4. Principle of fuzzy logic control [18]

Fuzzification will transform the input variables into fuzzy variables. For our study, we have two input variables namely the error $E(k)$ and the error variation $\Delta E(k)$. These variables will be denoted as Negative Large (NB), Negative Small (NS), Error Null (ZE), Positive Small (PS), Positive Large (PB) respecting the literature [13], [14]. These variations are defined by the following equations:

$$E(k) = \frac{\Delta P_{pv}}{\Delta V_{pv}} \tag{9}$$

$$\Delta E(k) = E(k) - E(k - 1) \tag{10}$$

Using equations (7) and (8) we obtain:

$$E(k) = \frac{P_{pv}(k) - P_{pv}(k - 1)}{V_{pv}(k) - V_{pv}(k - 1)} \tag{11}$$

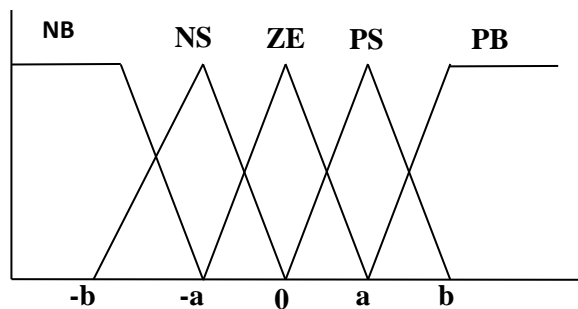


Fig. 5. Degree of membership of the variables

Inference from the literature [15], [16] will allow to define a logical relationship between inputs and outputs. Indeed, membership rules will be defined for the output as for the inputs. Thanks to these rules, table 1 of inference is drawn up

Table 1. Interference Matrix

$E/\Delta E$	NB	NS	EZ	PS	PB
NB	EZ	EZ	NB	NB	NB
NS	EZ	EZ	NS	NS	NS
EZ	NS	EZ	EZ	EZ	PS
PS	PS	PS	PS	EZ	EZ
PB	PB	PB	PB	EZ	EZ

At the end, the defuzzification will consist in carrying out the inverse operation of the fuzzification, in order to obtain a numerical value understandable by the external environment.

Finally, we obtain the following maximum power point tracking algorithm:

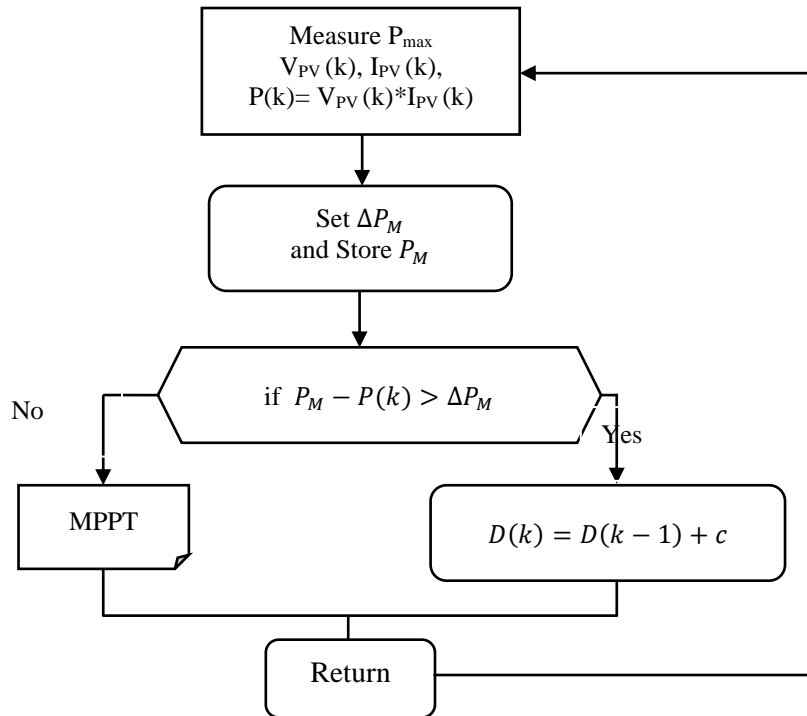


Fig. 6. Maximum power tracking algorithm

Therefore, the structure of our PV system controlled by the MPPT controller is as shown in Fig. 7.

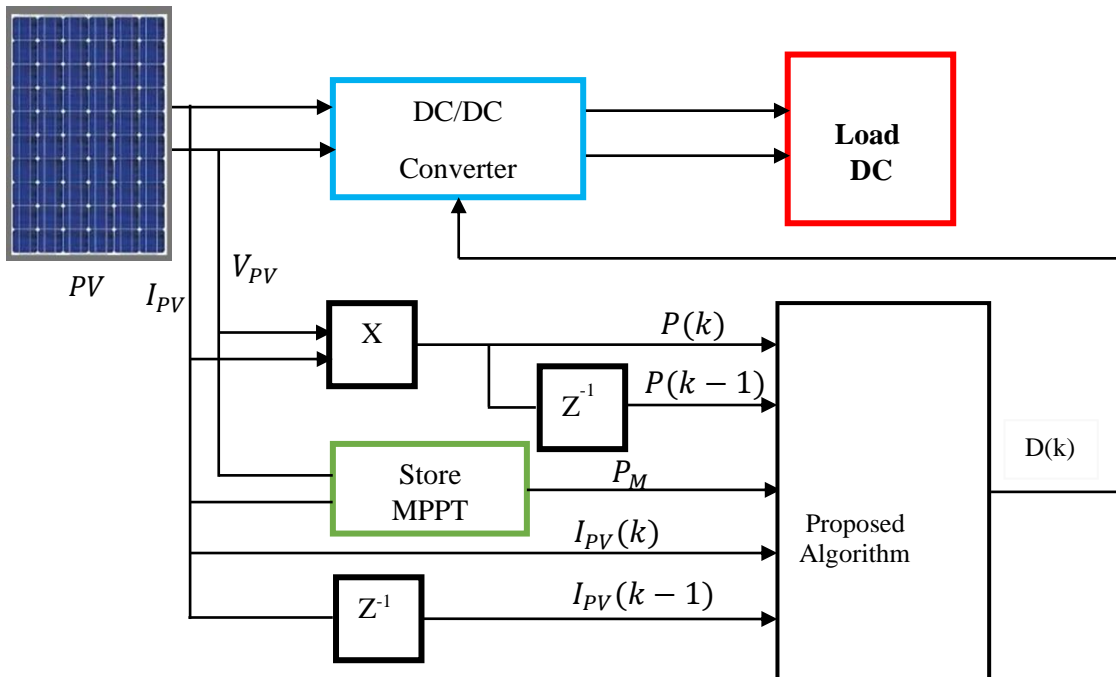


Fig. 7. Block diagram of the PV system with the MPPT controller

Each time after calculating $E(k)$ and $\Delta E(k)$, the fuzzy logic control will indicate the position that the maximum power point should take with respect to the load by respecting the degree of membership of the variables given in Table 1.

2.4 PRODUCTION OF ELECTRICAL ENERGY BY THE DIRECT CURRENT MOTOR - ALTERNATOR GROUP

2.4.1 BEHAVIOR OF THE DC MOTOR

The inductance of the DC motor creates a radial magnetic field in the air gap, directed along the radii of the armature. This magnetic field enters the armature on the side of the north pole of the inductor and leaves the armature on the side of the south pole of the inductor. When the armature is energized, a current flows through the conductors located under the same field pole (same side of the brushes) in the same direction. The conductors located under the other pole are subjected to a force of the same intensity and opposite direction and the two forces create a force couple that makes the armature rotate [17], [18].

2.4.2 ELECTRICAL EQUATIONS OF THE DC MOTOR

The electrical equations that govern the operation of our DC motor are:

$$V_{mpp} = U_a = R_a \cdot I_a + L_a \frac{dI_a}{dt} + \omega_r \cdot M_{fd} \cdot I_f \Rightarrow \frac{dI_a}{dt} = \frac{1}{L_a (U_a - \omega_r \cdot M_{fd} \cdot I_f - R_a \cdot I_a)} \quad (09)$$

The rotor of the machine has an electromagnetic torque, its expression is [19]:

$$C_{em} = P \cdot M_{fd} \cdot I_f \cdot I_a \quad (10)$$

The mechanical equation of the motor driving a resistive torque load is given by:

$$C_{em} - C_r = P \cdot M_{fd} \cdot I_a \quad (11)$$

$$C_{cem} - C_r = J \frac{d\Omega_r}{dt} + f \cdot \Omega_r \Rightarrow \frac{d\Omega_r}{dt} = \frac{1}{J(C_{cem} - C_r - f \cdot \Omega_r)} \quad (12)$$

In the operational domain assuming zero initial conditions, the motor equations are as follows:

$$V_{mpp}(p) = R_a \cdot I_a + pL_a(p) + E(p) \quad (13)$$

$$C_{cem}(p) - C_r(p) = J \cdot p\Omega_r(p) + f \cdot \Omega_r(p) \quad (14)$$

$$E(p) = K_m \Omega_r(p) \quad (15)$$

$$C_{cem}(p) = K_m \cdot I_a(p) \quad (16)$$

From equation (13) we can deduce the relationship between the supply voltage "Vmpp" and the back electromotive force "E(p)" which is given by

$$V_{mpp}(p) - E(p) = R_a \cdot I_a + pL_a(p) \quad (17)$$

With:

T_e : Electrical time constant;

K_m : Electromechanical coefficient;

J : Moment of inertia ($J=0.07 \text{ kgm}^2$);

f : Friction coefficient $f = 0.002 \text{ Nm/ (rad/s)}$;

C_r : Resistive torque;

K : General constant related to the rotating machine;

M : Motor torque;

R_a : Armature resistance;

L_a : Inductance.

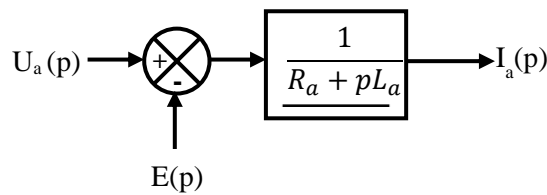


Fig. 8. Block diagram of the current loop

$U_a(p)$ corresponds to the voltage U of the PV one. From equation (16) we deduce the relationship between the armature current " $I_a(p)$ " and the electromagnetic torque " C_{cem} " (Fig. 9):

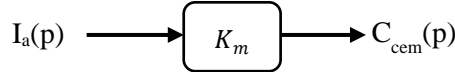


Fig. 9. Block diagram of the torque loop

From equation (14), we write equation (18) which represents the relationship between the speed of rotation " $\Omega_r(p)$ " and the useful torque " $\Omega_{cem}-\Omega_r$ " from which the diagram is given in Fig. 10.

$$C_{cem}(p) - C_r(p) = (J \cdot p + f) \cdot \Omega_r(p) \tag{18}$$

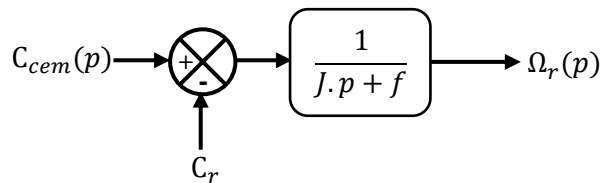


Fig. 10. Block diagram of the speed loop

The global transfer function given in equation 19 is obtained from equations (13), (14), (15), (16).

$$T(p) = \frac{\frac{K_m}{R_a \cdot f + K_m}}{(L_a \cdot J)p^2 + \left(\frac{L_a \cdot f + R_a \cdot J}{R_a \cdot f + K_m^2} \right)p + 1} = \frac{\Omega_r}{U_a} \tag{19}$$

This is the global block diagram of the DC MOTOR.

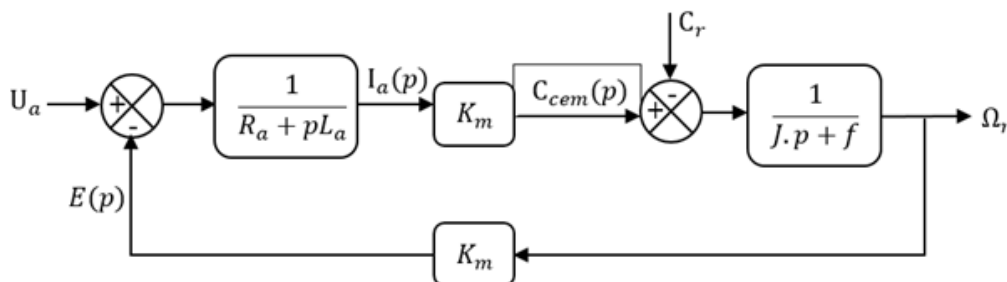


Fig. 11. Block diagram of the separately excited motor

These electrical equations allowed us to obtain the final model of the DC motor shown in Figure 11. It is from this model that we plan the simulation of the system. Here, in order to drive the alternator we need a good mechanical torque and a constant speed of the DC motor. For this, the energy produced by the PV system must be sufficient to keep the DC MOTOR running well.

This is how our DC MOTOR shunt is presented in the Simulink environment.

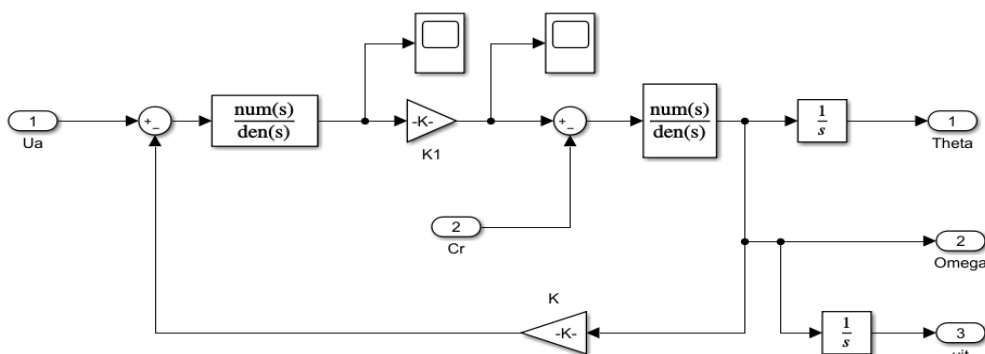


Fig. 12. Modeling of the DC motor

For this, the energy produced by the PV system must be sufficient to maintain the proper operation of the MCC.

This is how our MCC shunt looks like in the Simulink environment

2.4.3 THREE-PHASE ALTERNATOR

➤ Electromotive force

Our alternator receives mechanical power from the drive motor of the DC motor, whose expression is given by equation (10). The shunt excitation mode of the alternator is not studied in this article.

The effective value of the real electromotive force of a winding subjected to the magnetic field is given by the expression:

$$E = 2,22 \cdot K_d \cdot K_f \cdot f \cdot N \cdot \Phi \tag{20}$$

Where:

K_d : Distribution factor;

K_f : Form factor;

N : Number of conductors;

f : frequency of the network in Hertz (Hz);

Φ : magnetic flux in Weber (Wb).

$$\begin{aligned} e_1(t) &= E\sqrt{2} \cdot \cos(\omega t) \\ e_2(t) &= E\sqrt{2} \cos(\omega t - 2\pi / 3) \\ e_3(t) &= E\sqrt{2} \cos(\omega t - 4\pi / 3) \end{aligned} \tag{21}$$

➤ **absorbed power**

The absorbed and useful powers are those involved in the alternator. The absorbed power is the one supplied by the DC motor.

$$P_a = \Omega_s T_M = 2\pi N_s T_M \tag{22}$$

Where:

Ω_s : Rotational pulse in rad/s.

N_s : Speed in rpm.

T_M : Useful torque on the shaft in N.m.

As the alternator is not self-excited, the electrical energy absorbed by the excitation (rotor) must still be taken into account and this absorbed power becomes:

$$P_a = \Omega_s T_M + U_e I_e = 2\pi N_s T_M + U_e I_e \tag{23}$$

With:

I_e : excitation current;

U_e : excitation voltage.

The alternator provides useful electrical power P_U which depends on the load which is connected (influence of $\cos \phi$). In the case of the three-phase alternator, we have:

$$P_U = \sqrt{3}UI \cos \phi \tag{24}$$

With U , I and $\cos \phi$ respectively the line voltage, the current and the power factor delivered by the alternator.

2.4.4 CONTROL SYSTEM REGULATES THE POWER

The alternator is going to produce electrical energy in alternative form in three phase with neutral. The loads being resistive and inductive, we will regulate the active and reactive power of our system by a proportional-integral (PI) corrector.

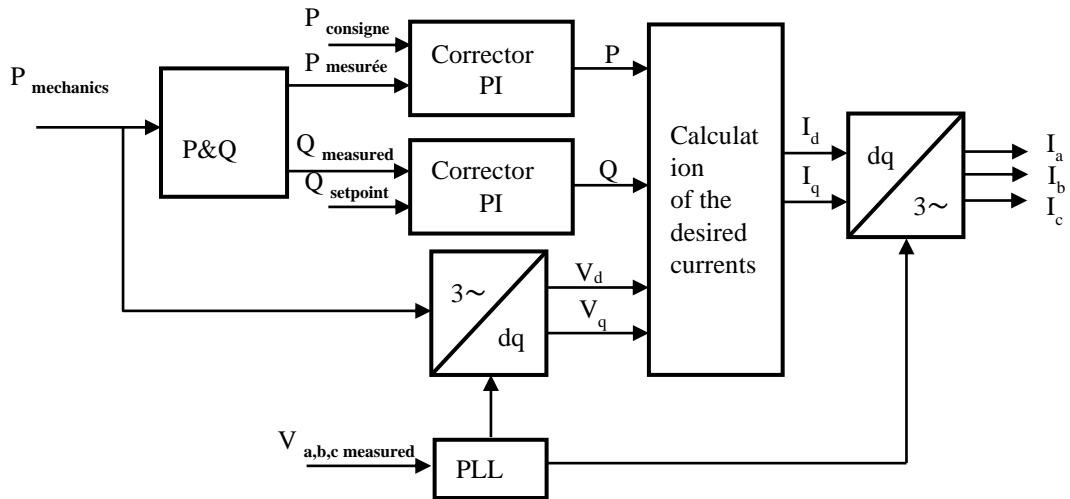


Fig. 13. Schematic diagram of the P/Q injection [20]

The current references are then calculated in the Park reference frame by the formula:

$$\begin{cases} I_d = \frac{2(PV_d + QV_q)}{3(V_d^2 + V_q^2)} \\ I_q = \frac{2(PV_q - QV_d)}{3(V_d^2 + V_q^2)} \end{cases} \quad (25)$$

Where P and Q are the reference powers of the generating system.

V_d and V_q are the direct and quadrature components of the voltage, measured at the operating point, in the Park reference frame.

Two PI correctors are in charge of regulating the active and reactive powers at their set value [25]. Therefore, there are two loops: the active power control loop and the reactive power control loop. First, we present the sizing study of the active power loop.

3 RESULTS AND DISCUSSION

Simulations were performed on the Simulink environment of Matlab, on the PV system, the MCC and the alternator. In this phase, we did not study the operation of the string protection devices, nor the limits of the battery discharge, nor the high inrush current of the MCC. Also, the excitation mode of the MCC and the alternator has not been addressed.

3.1 DC MOTOR WITHOUT RESISTIVE TORQUE

The DC motor is driven by the photovoltaic source, the model of the DC motor has been given above. Figure 12 shows the variation of current, torque and speed of the DC motor.

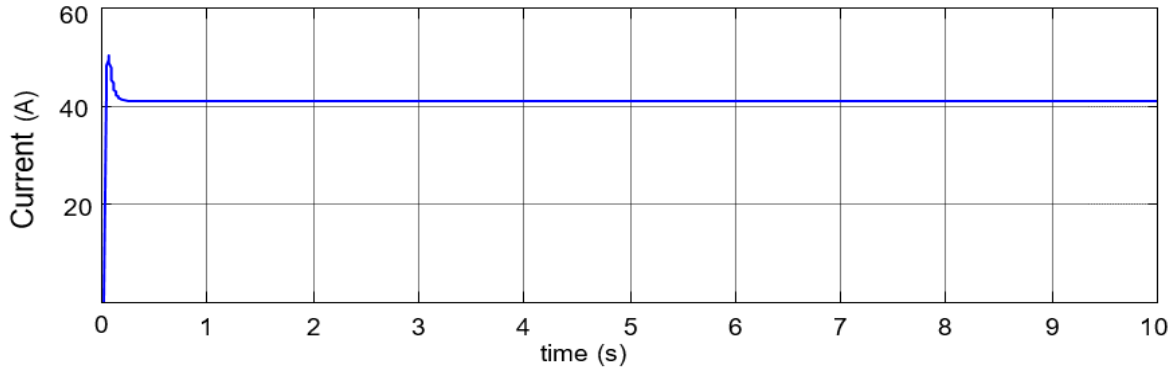


Fig. 14. Evaluation of the magnitude of the armature current of the (DC MOTOR)

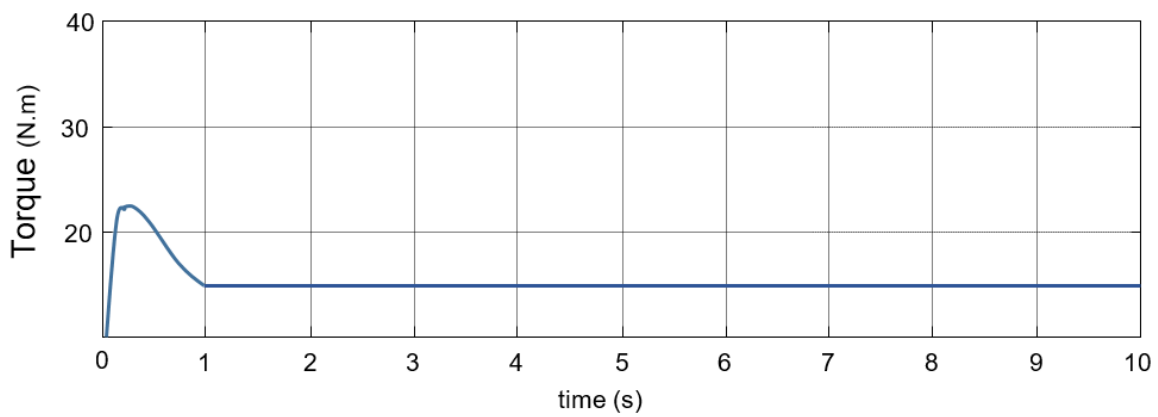


Fig. 15. Evaluation of the magnitude of the electromagnetic torque of the DC MOTOR

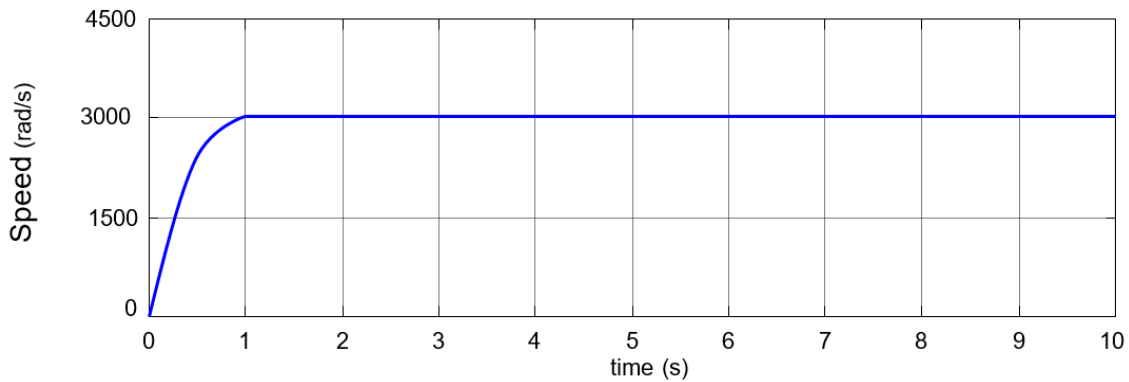


Fig. 16. Evaluation of the magnitude of the speed of DC MOTOR

Here we see that at 0.7s the current, electromagnetic torque and speed stabilize and remain constant at the value of steady state operation. This makes the protection elements provide more effort only in 0.07s.

3.2 VALUE IN TRANSIENT AND STEADY STATE

From the graphs obtained we take the maximum values presented in the following table 2:

Table 2. Parameter of the DC motor

Transient value		Value in steady state	
Ua	220 V	Ua	240 V
Ia	49 A	Ia	41 A
C_{em}	22 N.m	C_{em}	15 N.m
		ω_r	3000 rad/s

At this point, our study does not address the limitations of battery discharge or the high inrush current of the DC MOTOR. Moreover, we assume that the system is equipped with all its devices.

3.3 DC MOTOR WITH RESISTIVE TORQUE

We apply a resistive torque $C_r = 10$ N.m at time $T=3$ s to illustrate its influence on the speed, (Figure 17)

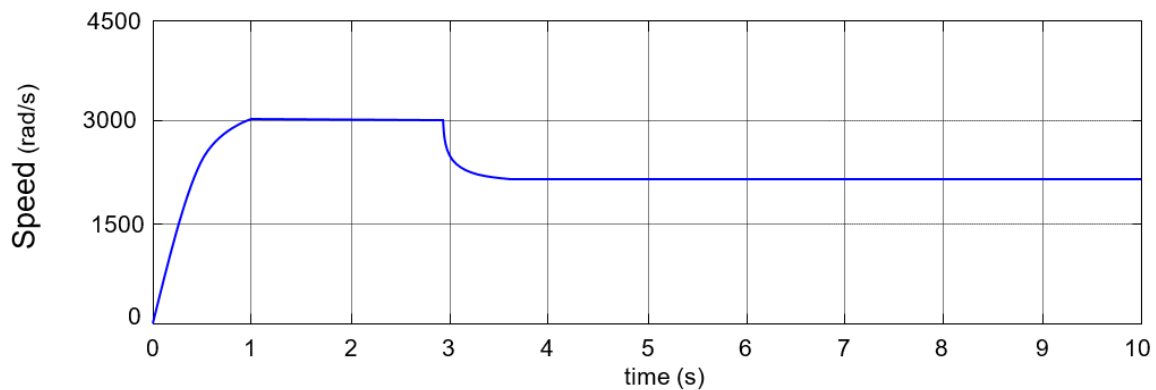


Fig. 17. Speed of the DC MOTOR with application of resistive torque

The output speed of the motor is applied to a resistive torque $C_r = 10$ N.m at the time $T=3$ s, we notice that the speed drops, which will change the operation of the DC MOTOR. This is why a speed controller (PI) was used to bring the speed of the DC MOTOR back to its reference speed regardless of the load applied.

3.4 DC MOTOR SPEED CONTROL

We are going to regulate the speed of the DC motor so that it remains at its reference value.

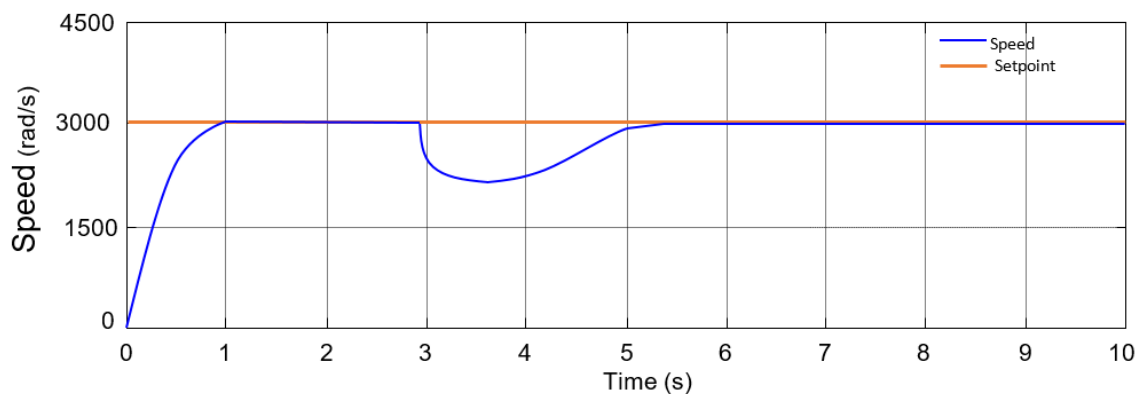


Fig. 18. Response of the speed with regulation

After a growth phase during the start-up period, the engine output speed stagnates from 0.7 seconds before decreasing at time $t = 3$ seconds to 115 radians per second. Thereafter, the speed of the MCC driving the alternator is constant. Thus, in anticipation of variations in the energy demand produced by the alternator, a speed controller (PI) is inserted to bring the speed of the MCC back to its reference speed regardless of the load applied.

Figure 18 shows the speed response with this control. It can be seen that the speed dropped after the torque was applied and then it returns to the reference speed. We conclude that the PI controller (proportional integral) plays a very important role on the system to be controlled (alternator) and also improves the performance of our machine (precision and stability).

3.5 SIMULATION OF THE PV SYSTEM

After simulating the independently excited DC machine and seeing its characteristics, we will connect it directly to the system. In order to have the necessary supply voltage and to satisfy the characteristics of the DC machine, the whole PV system has been simulated with a BOOST chopper. Figure 19 shows the whole PV system.

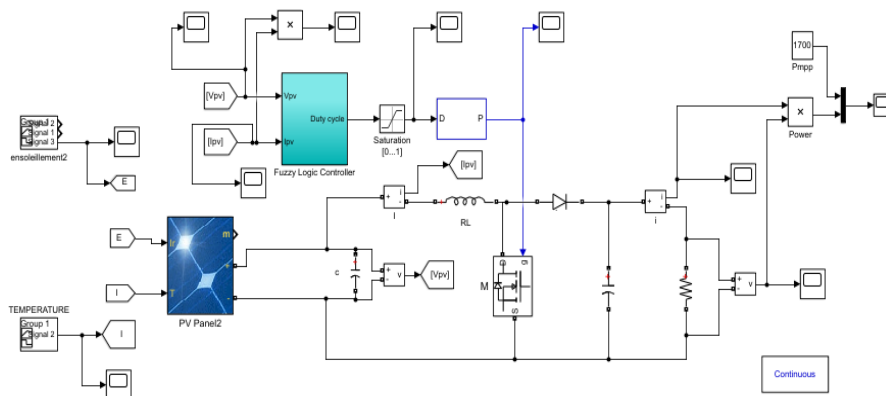


Fig. 19. Photovoltaic system

The (Figures 20, 21 and 22) represent the PV generator current and the DC-DC converter voltage and power output.

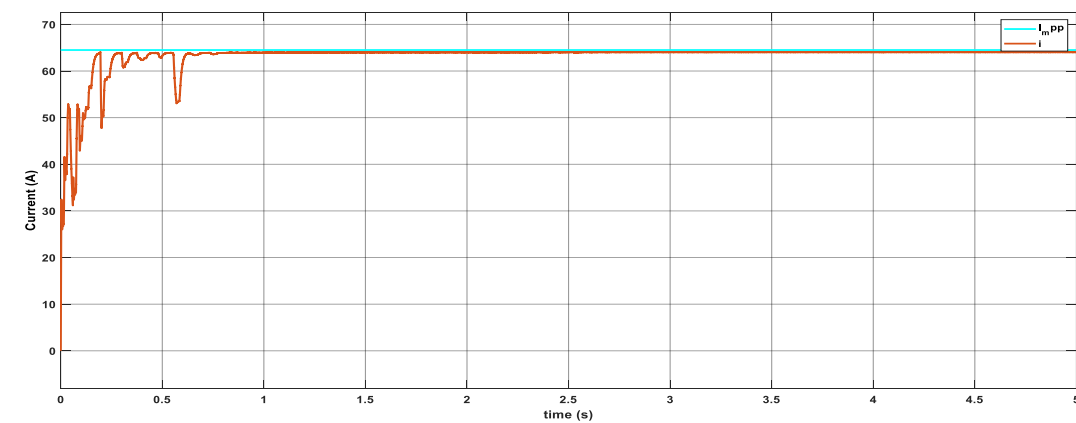


Fig. 20. Output current of the photovoltaic generator

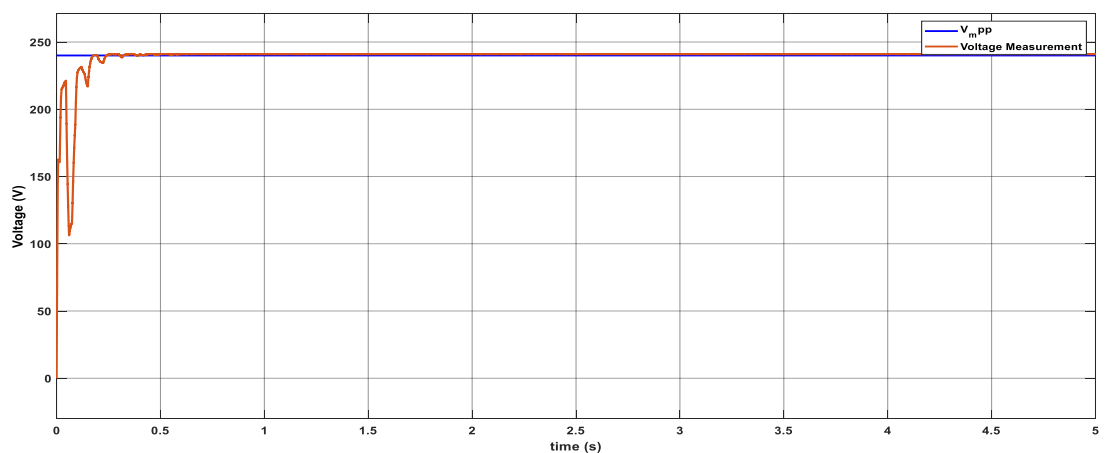


Fig. 21. Output voltage of the DC-DC converter

Figure 22 shows the evolution of the voltage generated by the PV panel at the output of the DC/DC converter for an illuminance of 1000W/m² and a temperature T=25°C.

As a general remark for the voltage, although we started the simulation with zero initial conditions, the MPPT control by fuzzy logic allowed us to find the nominal operating point of our load corresponding to the maximum power point of the panel.

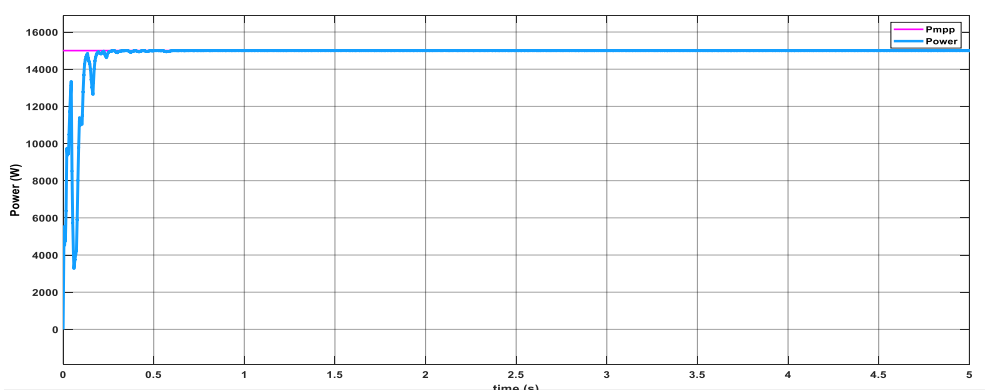


Fig. 22. DC-DC converter output power

Figure 22 shows the evolution of the voltage generated by the PV panel at the output of the DC/DC converter for an illuminance of 1000 W/m² and a temperature T = 40 °C.

➤ Interpretation of the results

The boost chopper provides a higher voltage at its output than the one provided by the photovoltaic generator. This allows us to power the DC motor and also to charge the batteries while keeping the same power, with a small decrease due to losses in the components. Here, the objective is to produce photovoltaic electric energy with a power of 14 kW. This power represents the maximum power. These results are satisfactory for the proper functioning of our system.

3.6 THE ENERGY PRODUCED BY THE ALTERNATOR

The synchronous alternator will produce electrical energy in three phases with neutral. Here the DC MOTOR is powered by a photovoltaic source.

Figure 23 shows the mechanical torque transmitted to the alternator by the DC motor, the current delivered by the alternator, the speed of rotation, the power and the electromagnetic torque of the alternator. From this curve, we can see that when the mechanical torque (the torque transmitted to the alternator) decreases, the current, the power produced and the electromagnetic torque of the alternator decrease abruptly and remain at a certain value while the speed decreases gradually.

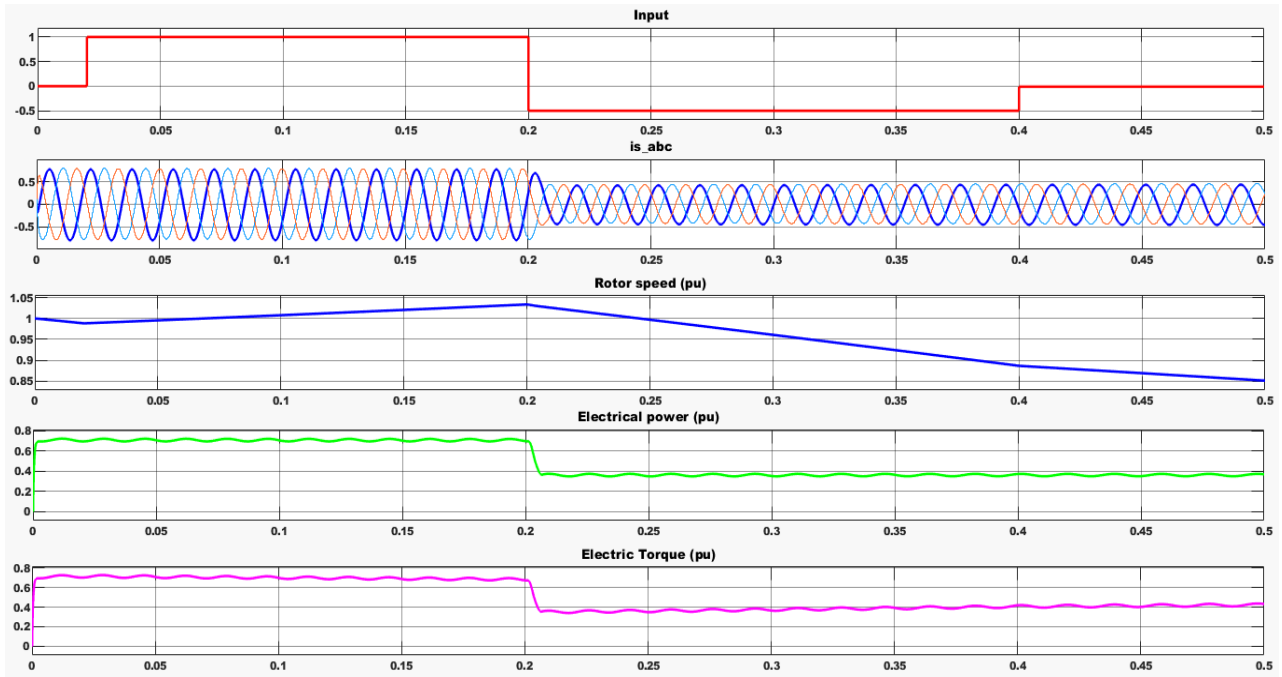


Fig. 23. Curve describing the characteristics of the alternator

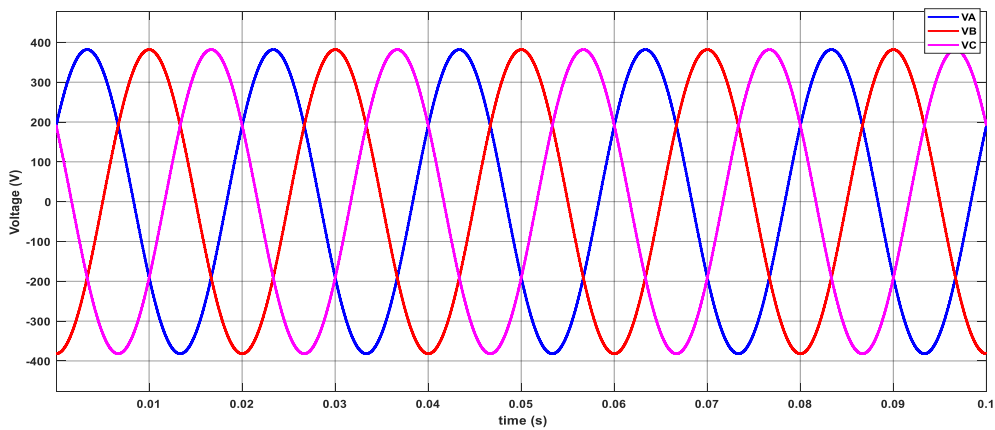


Fig. 24. Voltage curve of distributed generation without Regulation

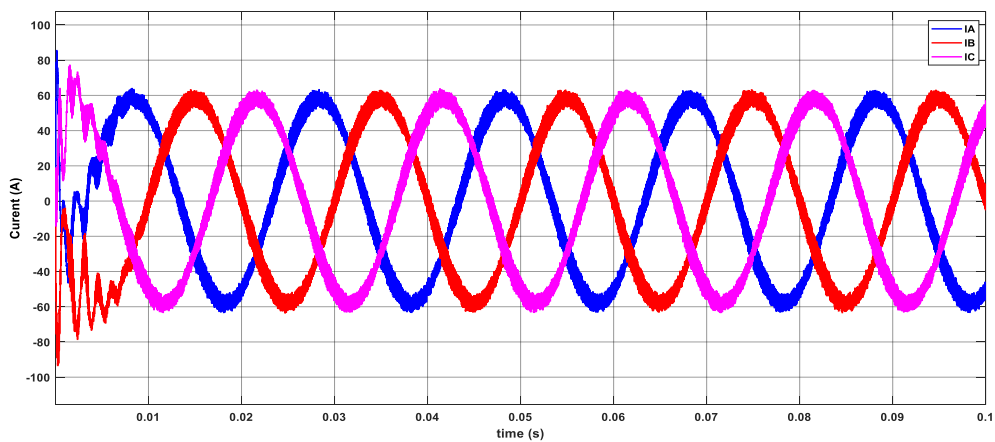


Fig. 25. Current curve of distributed generation without regulation

To make better use of this energy, we need to introduce a corrector and a regulation system to filter the energy at the output of the alternator.

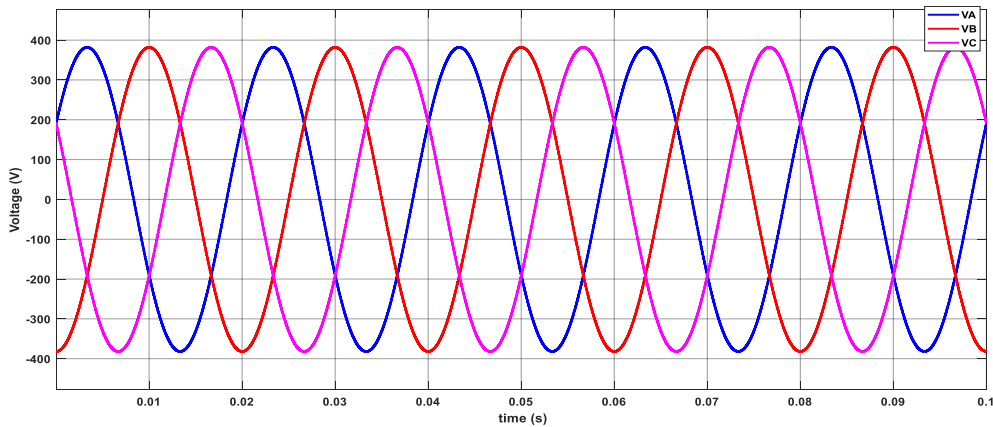


Fig. 26. Voltage curve of distributed generation with regulation

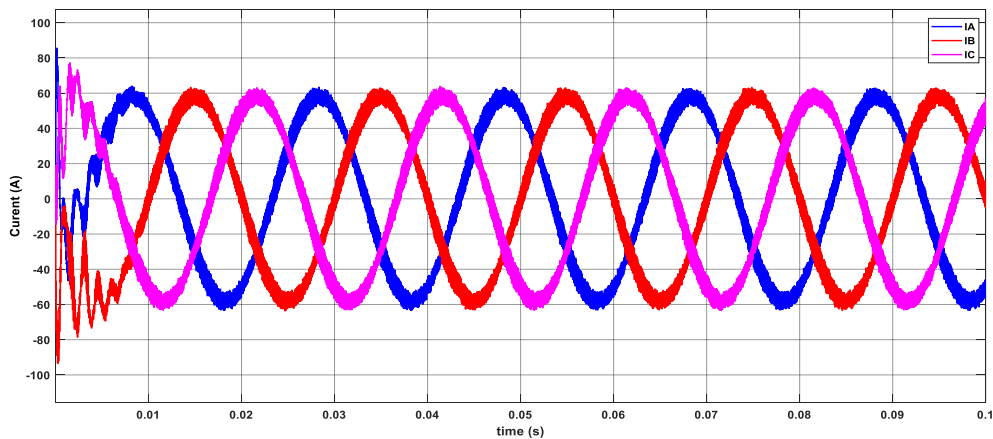


Fig. 27. Current curve of distributed generation with regulation

Thanks to the regulations, we obtain a more stable current and voltage from 0.005s. Indeed, the critical voltages of the previous simulations are avoided. Our DC MOTOR- generator system delivers an AC current of 63.5 A with an AC voltage of 380 V.

This energy produced by the DC MOTOR-generator is intended to supply a small town of 2,000 inhabitants. From the operating point of view, the load being considerable, when the PV system is connected directly to the load, it will require an equally important current. This will increase the number of photovoltaic panels and the storage batteries, so the production cost will be very high. On the other hand, our DC MOTOR-alternator only needs the power necessary to run the DC motor at its permanent speed in order to drive the alternator, which will produce an alternative power of 30 kW. With this energy, we will be able to supply this small city.

In our case, the rate of harmonic distortion of the voltage varies between [0.03 0.176] %, these values are smaller than the values of the rate of harmonic distortion of permissible voltages which is 5%. The frequency of the alternator is in an admissible range: $49.Hz \leq f_{alt} \leq 50.2Hz$. All these results are satisfactory and confirm the good functioning of our system necessary that the energy produced by the photovoltaic system can feed the DC motor well.

4 CONCLUSIONS

This paper is devoted to the optimization of renewable energy production sources. The objectives of this paper were first the extraction of the maximum power from the photovoltaic (PV) cells by the so-called intelligent control which is based on

fuzzy logic on the MPPT controller. Secondly, the production of electrical energy by an alternator driven by a DC motor, which is fed by DC current from the PV cells. Thus, the voltage, current and power signals from the PV cells vary during the period from 0 to 0.25 seconds with peaks of various amplitudes depending on the amount of electricity. From 0.25 seconds, these quantities are constant and maximum with a relative increase of 60%. These quantities were then exploited as parameters of the drive motor of the three-phase alternator. The voltages produced by the alternator are symmetrical with a low harmonic distortion rate of 0.76%. During our work, some aspects attracted our attention: the discharge of the batteries during the start-up of the MCC and its excitation mode, the integration of the excitation mode of the alternator in a wider regulation. All these aspects which have not been addressed are perspectives for future work.

REFERENCES

- [1] A.P.K. Yadav, S. Thirumaliah and G. Haritha, 'Comparison of MPPT Algorithms for DC-DC Converters Based PV Systems', *International Journal of Advanced Research in Electrical, Electronics and Instrumentation Engineering*, Vol. 1, N°1, 2012.
- [2] Ö. Çelik et A. Teke, « A Hybrid MPPT method for grid connected photovoltaic systems under rapidly changing atmospheric conditions », *Electr. Power Syst. Res.*, vol. 152, p. 194-210, nov. 2017, doi: 10.1016/j.epsr.2017.07.011.
- [3] S. Farajdadian et S. M. H. Hosseini, « Optimization of fuzzy-based MPPT controller via metaheuristic techniques for stand-alone PV systems », *Int. J. Hydrog. Energy*, vol. 44, no 47, p. 25457-25472, oct. 2019.
- [4] T. Noguchi, S. Togashi, R. Nakamoto, « Short-current pulse-based maximum-power-point tracking method for multiple photovoltaic-and-converter module system », *IEEE Trans. Ind. Electron.*, vol. 49, no 1, p. 217-223, feb. 2002.
- [5] Huang, C., Wang, L., Yeung, R.S.-C., Zhang, Z.J., Chung, H.S.-H. and Bensoussan, A. (2018) A Prediction Model-Guided Jaya Algorithm for the PV System Maximum Power Point Tracking. *IEEE Transactions on Sustainable Energy*, 9, 45-55. <https://doi.org/10.1109/TSTE.2017.2714705>.
- [6] A. de O. Ferreira, A. U. Brito, M. A. B. Galhardo, L. Ferreira, et W. N. Macêdo, « Modeling, control and simulation of a small photovoltaic-wind water pumping system without battery bank », *Comput. Electr. Eng.*, vol. 84, p. 106619, juin 2020, doi: 10.1016/j.compeleceng.2020.106619.
- [7] U. Yilmaz, A. Kircay, et S. Borekci, « PV system fuzzy logic MPPT method and PI control as a charge controller », *Renew. Sustain. Energy Rev.*, vol. 81, p. 994-1001, janv. 2018, doi: 10.1016/j.rser.2017.08.048.
- [8] F. Slama, « Amélioration de l'intégration des énergies renouvelables au réseau électrique (smart grid) », Thèse, 2021. [En ligne]. Disponible sur: <http://dspace.univ-setif.dz:8888/jspui/handle/123456789/3851>.
- [9] Y. S. Lim, J. Wong, M. S. S. Liew, et L. Y. A. Khaw, « Proportional integrator (PI) and fuzzy controlled energy storage for zero-power flow between grid and local network with photovoltaic system », *Sustain. Energy Technol. Assess.*, vol. 37, p. 100629, févr. 2020, doi: 10.1016/j.seta.2020.100629.
- [10] Lim, L.H.I., Ye, Z., Ye, J., Yang, D.Z. and Du, H. (2015) A Linear Method to Extract Diode Model Parameters of Solar Panels from a Single I-V Curve. *Renewable Energy*, 76, 135-142. <https://doi.org/10.1016/j.renene.2014.11.018>.
- [11] B. G. Jeannot, M. J. Jacques, et M. M. Jeannot, « Reliability of the MPPT Control on the Energy Parameters of a Photovoltaic Generator », *World J. Eng. Technol.*, vol. 8, no 3, Art. no 3, juill. 2020, doi: 10.4236/wjet.2020.83038.
- [12] J.-K. Shiao, Y.-C. Wei, et B.-C. Chen, « A Study on the Fuzzy-Logic-Based Solar Power MPPT Algorithms Using Different Fuzzy Input Variables », *Algorithms*, vol. 8, no 2, Art. no 2, juin 2015, doi: 10.3390/a8020100.
- [13] Afshan Ilyas, M. Rizwan Khan, Mohammad Ayyub, « FPGA based real-time implementation of fuzzy logic controller for maximum power point tracking of solar photovoltaic system » *Optik - International Journal for Light and Electron Optics* 213 (2020) 164668.
- [14] N. Patcharaprakiti, S. Premrudeepreechacharn, et Y. Sriuthaisiriwong, « Maximum power point tracking using adaptive fuzzy logic control for grid-connected photovoltaic system », *Renew. Energy*, vol. 30, no 11, p. 1771-1788, 2005.
- [15] S. Farajdadian et S. M. H. Hosseini, « Optimization of fuzzy-based MPPT controller via metaheuristic techniques for stand-alone PV systems », *Int. J. Hydrog. Energy*, vol. 44, no 47, p. 25457-25472, oct. 2019.
- [16] B. Mbarki, F. Farhani, et A. Zaafouri, « Comparative study of some Maximum Power Point Tracking algorithms », in 2019 International Conference on Signal, Control and Communication (SCC), déc. 2019, p. 145-149, doi: 10.1109/SCC47175.2019.9116145.
- [17] K. Lahouar et A. Silini, « Etude Comparative de la Commande PID classique et la Commande d'ordre fractionnaire : Application à un Moteur à Courant Continu », Thesis, Univ M'sila, 2020. [En ligne]. Disponible sur: <http://localhost:8080/xmlui/handle/123456789/21572>.
- [18] B. Dich et N. Cherigui, « Etude d'une commande d'un moteur à courant continu », Thesis, Mme.S.BOURI, 2020. [En ligne]. Disponible sur: http://thesis.essa-tlemcen.dz:8080/xmlui/handle/STDB_UNAM/77.
- [19] S. Messalti, « Analyse de la stabilité transitoire des réseaux de transport a courant continu en haute tension (HVDC-FACTS) », Thesis, 2018. [En ligne]. Disponible sur: <http://dspace.univ-setif.dz:8888/jspui/handle/123456789/2253>.
- [20] I. Zoric, M. Zabaleta, M. Jones, et E. Levi, « Techniques for power sharing between winding sets of multiple three-phase machines », in 2017 IEEE Workshop on Electrical Machines Design, Control and Diagnosis (WEMDCD), avr. 2017, p. 208-215. doi: 10.1109/WEMDCD.2017.7947748.